Highly Oriented Molecular Ag Nanocrystal Arrays

Steven A. Harfenist,[†] Z. L. Wang,*[,§] Marcos M. Alvarez,[‡] Igor Vezmar,[†] and Robert L. Whetten*[,†]

Schools of Physics and Chemistry, and Microelectronics Research Center, Georgia Institute of Technology, Atlanta, Georgia 30332-0430, and Schools of Materials Science and Engineering, Georgia Institute of Technology, Atlanta, Georgia 30332-0245

Received: June 14, 1996[⊗]

Orientational ordering of faceted nanocrystals in nanocrystal arrays has been directly observed for the first time, by use of transmission electron microscopy imaging and diffraction to resolve the structure of thin molecular-crystalline films of silver nanocrystals passivated by alkylthiolate self-assembled monolayers. The type of ordering found is determined by the nanocrystal's faceted morphology, as mediated by the interactions of surfactant groups tethered to the facets on neighboring nanocrystals. Orientational ordering is crucial for the understanding of the fundamental properties of quantum-dot arrays, as well as for their optimal utilization in optical and electronic applications.

Introduction

Materials composed of metal nanocrystals are of great current interest because of the enhancement in optical and electrical conductance properties that arises from confinement and quantization of conduction electrons within a small volume.[1] Recent investigations have revealed interesting and potentially useful properties, including extremely large optical polarizabilities,[2] nonlinear electrical conductance[3] of nanocrystal arrays that also have small thermal activation energies (∼0.1 eV),[4] and Coulomb-blockade and -staircase phenomena in the conductance through single nanocrystals persisting to unusually high temperature.[5,6] The optimal manifestation of these properties depends on the nanocrystal material's quality, encompassing uniformity in size, shape (or crystallite morphology), internal structure, surface passivation, and spatial orientation of the nanocrystals. The significance of the last of these is apparent from the fact that nanometer-scale crystallites preferentially have well-faceted polyhedral shapes, in which the vertexes and the edge and face centers point along crystallographic axes of the nanocrystal's internal lattice.[7,8] Consequently, all transport and optical properties are orientation dependent for a single nanocrystal and, in the case of a condensed nanocrystal array or superlattice, are sensitive to orientational order.

High-quality nanocrystal solids have become possible because of a remarkable set of facts,[9] namely, that nanocrystals passivated by suitably matched surfactants can retain their ideal core morphology and yet behave as stable macromolecules, i.e., can reversibly form solutions in solvents appropriate to the surfactant tail groups and be evaporated rapidly to form a molecular vapor,[10] that they can be separated from mixtures into highly purified substances composed of a single size and shape, and that they can condense to form crystalline *molecular* solids with high translational (center-to-center) order.[11,12] It is in such molecular crystals that the question of orientational order becomes crucial. Generally, crystals formed from high-symmetry molecules are orientationally ordered, i.e., the molecular axes are co-oriented with respect to each other and with respect to the crystallographic axes of the lattice, only below an orientational ordering temperature.[13] Despite their distinctly nonspherical, polyhedral shape, it is not clear whether passivated nanocrystals interacting mainly through their surfactant groups will form highly oriented molecular crystals.

Recently, limited evidence for nanocrystal alignment has been provided by X-ray diffraction patterns obtained on films of diverse nanocrystal materials[11] and by direct observation of co-aligned nanocrystal lattice planes in a very thin film.[12] These results are insufficient to reveal the packing of faceted particles and their surfactant groups, and even in the most favorable interpretation would establish only alignment rather than orientation. Here we report clear evidence of high molecular orientational order in nanocrystal lattices, in the form of direct observations of co-oriented shapes, lattice fringes, and surfactant density profiles, in thin crystalline films of nanocrystal silver (Ag) molecules. Our results also suggest a directionality in the distribution of surfactant chains, which serve as the *inter*molecular bonds connecting nanocrystals.

Methods

The molecular silver nanocrystals under investigation here are from the same class of materials that has enjoyed rapidly growing interest in the past several years.[3−5,10,12,14,15] They are charge-neutral entities comprised entirely of an elemental metal (Au, Ag, Pt) core and a dense mantle of alkylthiol(ate) surfactant groups, normally straight-chain n-$CH_3(CH_2)_mS$, and share, by all tests to date, the properties that have made their extended-surface analogues, the so-called self-assembled monolayers (SAMs),[16] one of the best-studied surface material systems. For example, it has recently been shown that nanocrystal gold molecules of this class with small (<3 nm diameter) cores form preferentially in certain distinct sizes, which can be separated from each other as highly purified (macro)molecular materials.[10] These passivated metal nanocrystals can be made in several ways;[17] an aerosol processing approach[18] has been used here because of the higher reactivity and air-sensitivity of Ag and the desirability of high-temperature annealing. Elemental Ag is evaporated at temperatures ranging from 1200 to 1500 K into a flowing, preheated atmosphere of ultrahigh-purity helium. The flow stream is cooled over a short distance (and flow time) to ca. 400 K, stimulating growth of nanocrystals in the desired size range, here ca. 4−6 nm. Growth is abruptly terminated

[†] School of Physics.
[‡] Schools of Physics and Chemistry, and Microelectronics Research Center.
[§] Schools of Materials Science and Engineering.
* To whom correspondence should be addressed.
[⊗] Abstract published in *Advance ACS Abstracts,* July 15, 1996.

S0022-3654(96)01764-9 CCC: $12.00

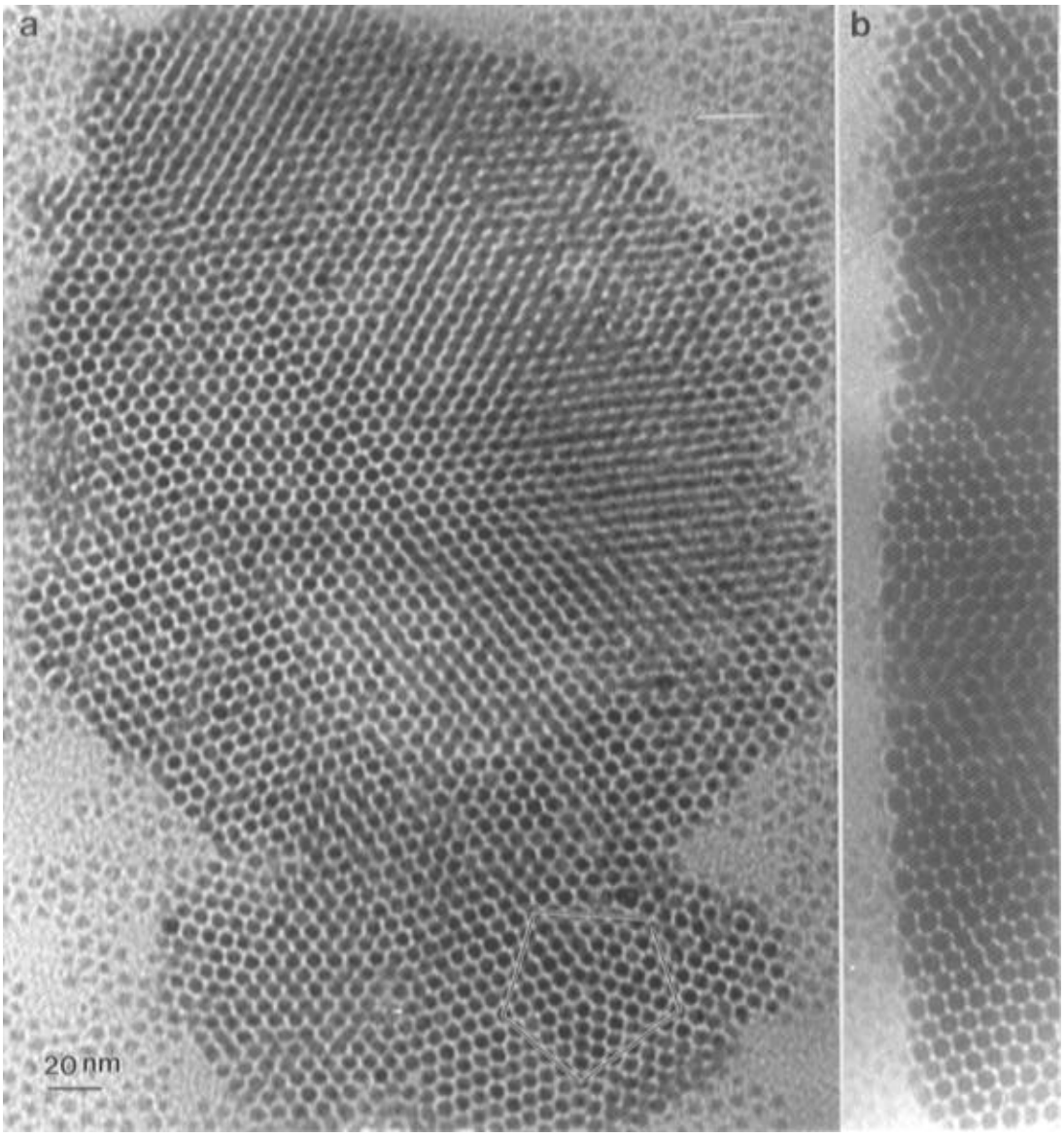

Figure 1. Typical low-magnification TEM images of Ag nanocrystal arrays viewed along $[110]_s$, showing (a) an entire thin crystal (with a multiply twinned region marked at lower right) and (b) the facet edge of an extended array.

by expansion through a conical funnel accompanied by dilution in a great excess of cool helium. Subsequent steps may include reheating (annealing) of the separated nanocrystals and etching and passivation by molecular vapors introduced downstream. Because alkylthiols have been found to etch noble-metal surfaces under mild conditions,[18] we have found it sufficient to co-condense the flowing nanocrystals in a solution or film with a great excess of alkylthiol molecules, which in the present case are dodecanethiols (C_{12} chains). Precautions must be taken to avoid air contamination until the etching and passivation processes are complete, otherwise the passivated nanocrystals have insufficient stability against oxidation and irreversible coagulation. Depending on conditions, most of the material produced is soluble in nonpolar solvents, from which excess surfactant can be removed. The soluble material is found to consist entirely of nanocrystal Ag molecules (NCAMs), and a survey of properties by transmission electron microscopy (TEM), X-ray diffraction, optical spectroscopy, and other diagnostics are consistent with a material analogous to that described for Au.[12]

Here we concentrate on the microstructure of the molecular crystals formed by reversible condensation of NCAMs from solution, as observed by TEM and electron diffraction (ED). A Hitachi HF-2000 cold-field emission gun TEM (200 kV) has been used to perform imaging and diffraction experiments. Each TEM specimen is prepared by depositing a highly concentrated drop of toluene solution of NCAMs on an ultrathin amorphous carbon film substrate and allowing it to dry slowly in air prior to TEM observations. Nanocrystal superlattices, such as those shown in Figure 1, appear on the carbon film, in the form of highly oriented thin crystalline films, whose lateral dimensions can be as large as 1 μm and are frequently bounded by straight edges consistent with reversible crystal growth. In this procedure, no prior separation of NCAMs according to size (or shape) is performed. Instead, it is found that each microcrystal exhibits a precisely defined and generally distinct (super)lattice constant, consistent with a powerful tendency toward segregation by size (and shape).[20,10]

Results and Discussion

Our first objective has been to establish the packing structure of the nanocrystal superlattice. Figure 2a shows a TEM image of an ultrathin (monolayer) film of 5.0 nm diameter NCAMs (6.4 ± 0.2 nm center-to-center spacing), in which 2-D close-packing is deduced from the clear 6-fold symmetry. The image

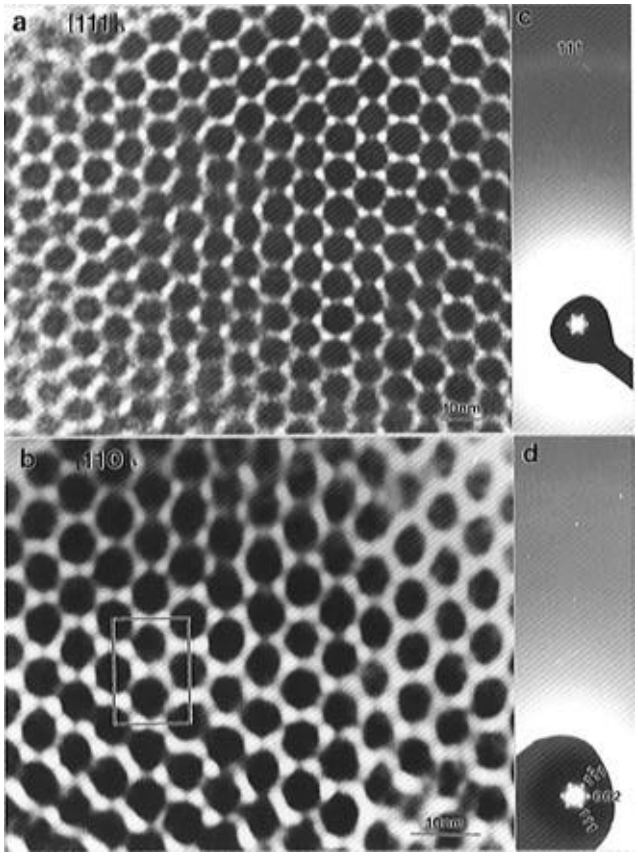

Figure 2. (a) 2-D close-packing and (c) $[110]_s$ TEM images and (b) and (d) corresponding electron diffraction patterns, respectively, obtained on thin films of nanocrystal Ag molecules, establishing the fcc packing structure of the multilayer superlattices. The Ag {111} reflection ring is seen in (c), which serves as an absolute calibration for determining the lattice constant of the superlattice, $a_s = 10.4 \pm 0.3$ nm. The solid line in (b) indicates the $[110]_s$ unit cell of the superlattice.

is dominated by the plane-projected arrangement of the nanocrystal cores, because of the much greater scattering power of Ag over the lighter elements (S, C, H). The electron diffraction pattern obtained from this region reveals the periodic structure of the nanocrystal lattices and also provides an absolute calibration of the superlattice constant, because the fcc-Ag {111} ring is recorded simultaneously in the same photograph (Figure 2c). Although this monolayer shows good translational ordering, it is insufficient to determine the kind of 3-D packing that will occur, because such $[111]_s$ planes are common to the fcc, bcc, diamond and hexagonal close packed (hcp) types. [The subscript s denotes the nanocrystal superlattice, to distinguish it from the reflections of atomic lattice of elemental Ag.] In this case, the $[110]_s$ diffraction pattern is indispensable, because it can unambiguously discriminate fcc from bcc and hcp, assuming that diamond packing of NCAMs is implausible. For multilayer films, the TEM image and the corresponding diffraction pattern (Figure 2b,d) confirms that the superlattice has the fcc structure. Such $[110]_s$-oriented films are the most frequently observed structure in our specimens and are very advantageous, as described previously,[11] in that the projection from individual columns of nanocrystals can be viewed without obstruction by neighboring columns, allowing one to clearly view a projected shape of the nanocrystals, as we now describe.

Our second objective has been to establish a relationship between this 3-D superlattice structure and the orientation of the NCAMs within it. Figure 3a,c are two TEM images recorded from the same specimen region under differing defocus conditions. Three striking features are observed. First, the superlattice contains "coherent" $\{200\}_s$ twin (T) and $\{111\}_s$ stacking fault (SF) structures. Although the $\{111\}_s$ stacking fault are common in dense fcc structures (elemental solids or crystals of spheres), the $\{200\}_s$ twins are very unusual; close examination shows that the (projected) nanocrystal shape is modified across the twin boundary, accompanying the transformation in superlattice orientation. Second, profiles of the faceted structure of the NCAM cores can be seen in the image recorded at the condition close to in-focus (Figure 3a,b), and the co-aligned arrangement of these projected shapes is apparent, in contrast to the results of Murray et al.,[11] which show only circular or elliptical profiles. The majority of the nanocrystal profiles observed are consistent with the truncated octahedral (TO) morphology, which exposes {100} and {111} facets, as described previously.[21] Viewed along [110], two {100} facets and four {111} facets are projected *edge-on* (Figure 3b). This establishes the orientational relationship between the NCAM core's lattice and the superlattice as $[110] \parallel [110]_s$ and $[002] \parallel [1\bar{1}0]_s$. Third, the image recorded at the out-focus condition exposes a weblike pattern of directional "contacts" among neighboring NCAMs, as indicated by dotted lines in Figure 3d, where the Ag cores are in dark contrast and the bright spots are channels enclosed by regions of enhanced density of surfactant chains. By comparison with Figure 3b, one can see that these dense regions interconnect between *facets* of Ag cores rather than edges or vertexes. It is therefore natural to suppose that the overlap of surfactant groups emanating from facets on neighboring nanocrystals serves as the prime contact which holds, or "bonds", and orients the particles in their 3-D superlattice. We further propose that materials of this special type be called "highly oriented molecular (Ag) nanocrystal arrays", HOM(A)NAs.

A precise orientational relationship between nanocrystal core lattices and the superlattice has been determined from a high-resolution lattice image (Figure 4) recorded on a very thin film (two layers) for which the electron beam is parallel to $[110]_s$, and the {111} lattice fringes of the Ag cores are clearly resolved. [This image has been recorded using a large objective aperture, so that phase contrast dominates and hence is insensitive to the nanocrystal shape; orientational fluctuations induced by focused electron-beam irradiation have also degraded the contrast in the image.] By tracing the $\{111\}_s$ planes of the superlattice, one finds a striking feature: the {111} lattice fringes of the Ag cores (as indicated by arrowheads) consistently show a small deflection (in the same sense) from the $\{111\}_s$ planes of the superlattice, thus defining a preferred orientational angle, α. A histogram of the experimentally measured angles is given in the inset, from which a value of $\alpha = 16 \pm 5°$ is obtained.

Working from all these experimental observations, we have constructed a 3-D structural model (Figure 5b) of the packing and orientational relationships in the HOMANAs observed, where each NCAM core is represented by a truncated octahedral (TO) shape (Figure 5a), consistent with the information provided by Figure 3a,b. Any variation in particle size and shape may introduce significant strain to the superlattice, and so this model is only an idealized representation of the practical situation. The model is generated by orienting the TO polyhedra according to the relationships established by the TEM images in Figures 3 and 4. Clearly, this orientation of objects of cubic symmetry within a cubic lattice breaks the lattice symmetry; hence, the faceted structure of the Ag cores could result in different lengths of the *a*, *b*, and *c* axes of the superlattice. Because of this loss of symmetry, the faceted structure of the nanocrystals produces inequivalent projected images when viewed along $[110]_s$ and $[1\bar{1}0]_s$ (Figure 5c,d). As viewed along $[110]_s$, the [110] orientation of the Ag nanocrystal is parallel to the $[110]_s$ of the

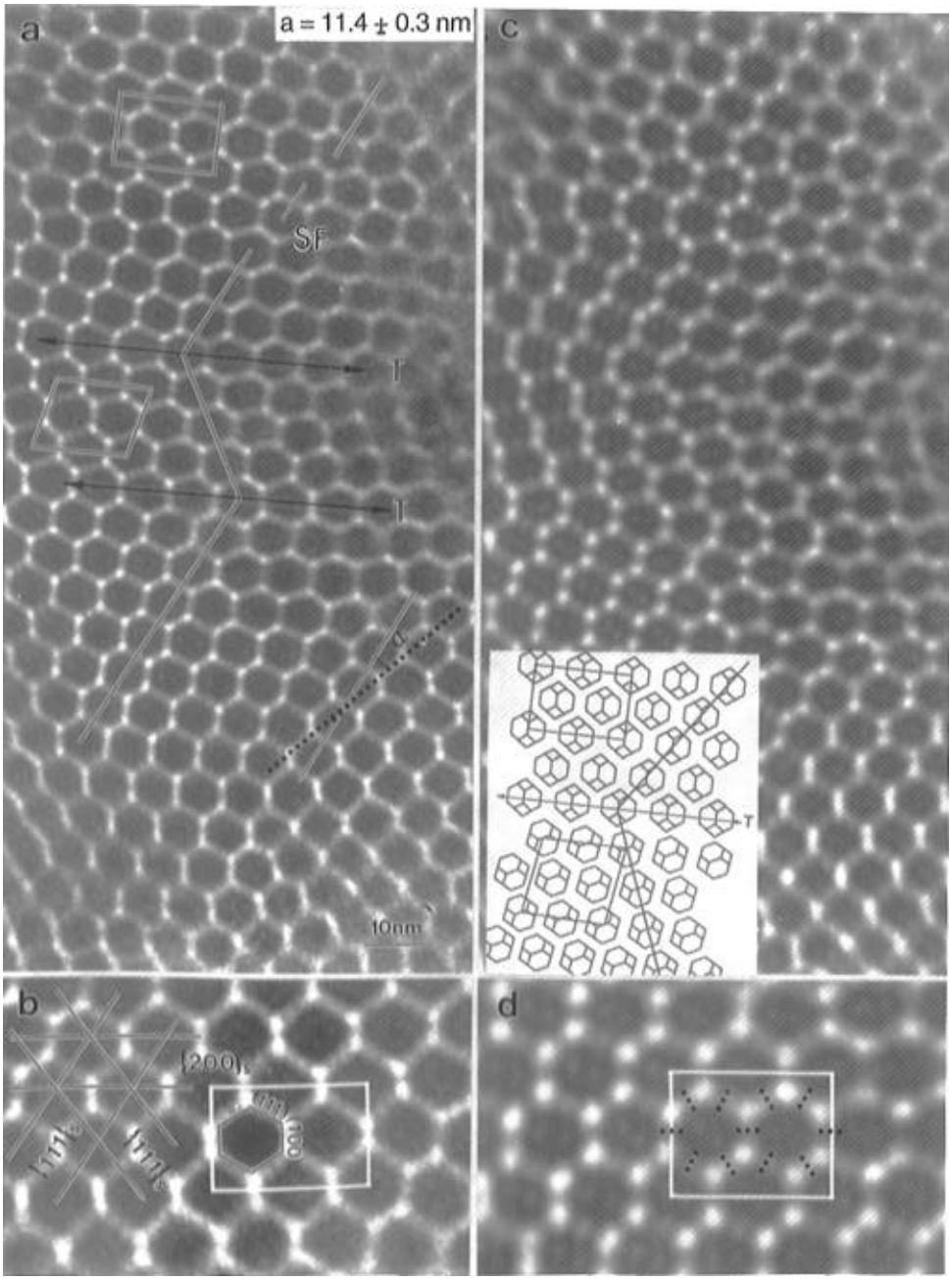

Figure 3. $[110]_s$ TEM images recorded from the a single region of a film under (**a**) in-focus and (**c**) out-of-focus conditions, showing the faceted shape and the directional intermolecular bonds of the particles. The dark lines indicate twin (T) planes and the white−dark lines indicate the rotation of the $\{111\}_s$ plane across the twin plane and the region with stacking faults. An angle, α, is indicated which measures the projected orientation between the {111} facet of a nanocrystal (dotted line) and the $\{111\}_s$ plane of the superlattice. A structural model for the formation of $\{100\}_s$ twins in the fcc superlattice is inset in (c) according to the structure model to be given in Figure 5b. (b) and (d) are enlarged TEM images selected from (a) and (c), respectively, showing the relationship of the {111} and {100} facets of the truncated octahedron particles to the projected unit cell (white lines) of the superlattice. The dotted lines in (d) indicate the directional intermolecular contacts formed by the groups of surfactant chains from facets on neighboring nanocrystals.

superlattice (Figure 5c), where four {111} and two {100} facets of the particle are parallel to the electron beam, in correspondence to the experimental image shown in Figure 3b. This model can also account for the multiply twinned region marked in Figure 1a. As viewed along $[1\bar{1}0]_s$, two of the {100} facets of the particles are perpendicular to the incident beam direction (Figure 5d), in which case each profile is octagonal. Considering also the strong Fresnel fringes near the edge of the particles, these profiles will have almost circular shapes in the TEM images, such as those shown in Figure 2b.

From the 2-D projected model in Figure 5c, an angle $\alpha = 19.4°$ is calculated between the {111} facet (as indicated) of the nanocrystal with the $\{111\}_s$ plane of the superlattice. This is the angle implicated from core orientations in the images shown in Figure 3b and established, by the high-resolution TEM image shown in Figure 4, to be $16 \pm 5°$. By contrast, the $[hkl] \,||\, [hkl]_s$ orientation of nanocrystal to superlattice axes would have necessitated $\alpha = 0$.

However, it is not immediately clear within this model why only one set of fringes is observed in each nanocrystal, rather than the two which must appear in the image if the cores are oriented with their [110] axes exactly parallel to the incident beam direction (Figure 5c). To account for this asymmetry and for other observations, we return to the image shown in Figure 3d, revealing the alignment of the intermolecular "contacts" with respect to the nanocrystal facets (Figure 3b). Specifically, we

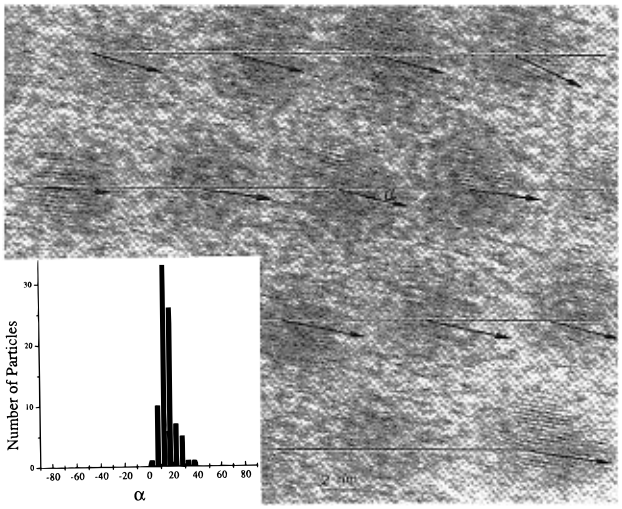

Figure 4. High-resolution TEM image recorded from a thin NCAM film viewed in the $[110]_s$ direction. The markings indicate the angular relationship (α) between the {111} lattice fringes of the Ag particles with the $\{111\}_s$ planes of the superlattice (indicated by white−dark solid lines). The inset is a histogram of α values measured from the experimental images.

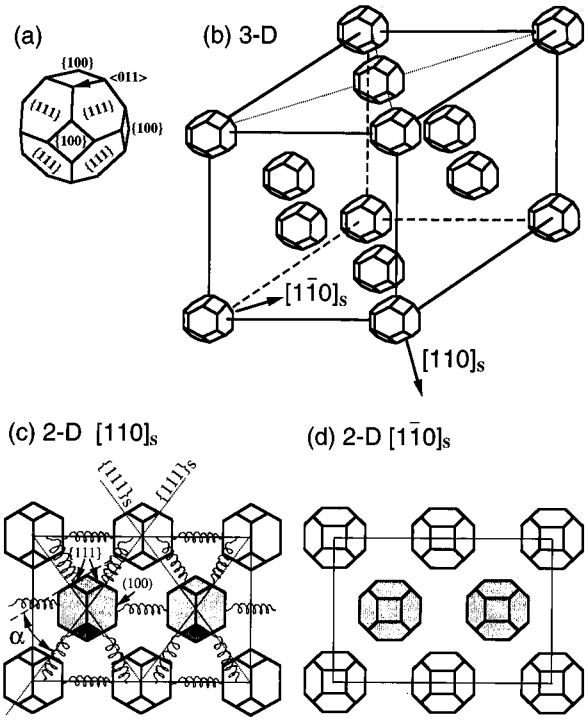

Figure 5. (a) Diagram of the truncated octahedron (TO) morphology of the Ag nanocrystals, with the {111} and {100} facet structure and ⟨011⟩ direction designated. These constitute the cores of the molecules forming the highly oriented nanocrystal lattices. (**b**) A schematic model of the fcc packing of the TO Ag cores and following the orientational relations of [110] || $[110]_s$ and [002] || $[1\bar{1}0]_s$. (c,d) The $[110]_s$ and $[1\bar{1}0]_s$ projections of the model shown in b. The shaded polyhedra are out-of-plane by a distance ($\sqrt{2}/4$) a. In (c), the angle α is indicated corresponding to that shown in Figure 3a. The intermolecular interactions are represented by coils that interconnect the {111} facets with {111} facets on neighboring nanocrysals and {100} with {100} facets. In these illustrations, the size of the Ag nanocrystals is reduced relative to their spacing, to permit a view of the distribution of nanocrystal cores throughout the entire cell.

propose that the chainlike tails of the surfactant molecules, whose heads are packed compactly over the nanocrystal surface, pack themselves into discrete groups directed radially outward from each {111} or {100} nanocrystal facet. The short-range (van der Waals) attraction between such groups from facets on

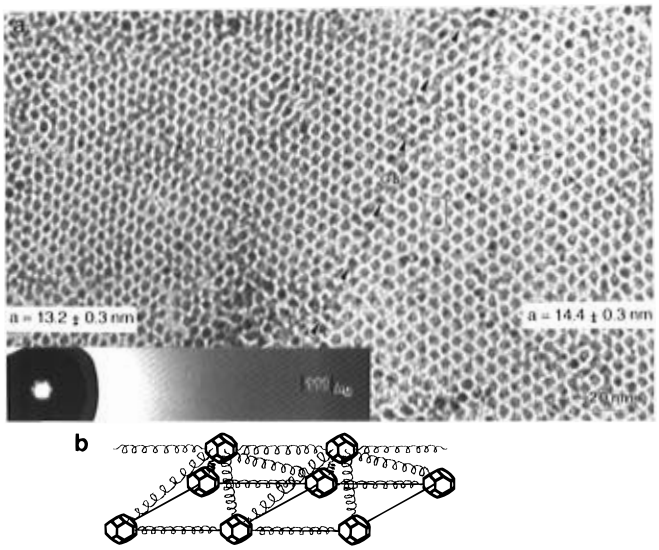

Figure 6. (a) TEM image showing a two-domain $[110]_s$ bilayer structure. The electron diffraction pattern recorded from the region is inset. The lattice constants for each region is indicated. (b) A structural model for the $[110]_s$ bilayer HOMANL, where the coils represent the intermolecular bonds.

two co-aligned neighboring nanocrystals may then constitute intermolecular "bonds", shown schematically as coils in Figure 5c. With a surfactant chain-length of only ~1.5 nm, these interactions naturally reach only the (12) nearest neighbors, and yet the distance of closest approach between the surfaces of adjacent nanocrystals, as determined by inspection of TEM images and evaluation of full 3-D models, is much less than 2 × 1.5 nm (the bilayer thickness assuming no interpenetration), consistent with substantial interdigitation along the directions of closest approach.[9,10] The coils should tend to align the two bond connected facets (Figure 5c), resulting in a slight tilt or twist in the orientation of the particle. This is the likely reason that only one set of {111} fringes are seen in the high-resolution TEM image, because a small tilt drastically reduces the visibility of the other set of {111} fringes.

[By contrast, Luedtke and Landman[15] have described theoretically a very different kind of surfactant group ordering that occurs in very small nanocrystals (<2 nm) passivated by relatively long alkyl chains (C_{12}), in which the surfactant groups from several facets of a single nanocrystal are "bundled" together into a single compact group; in a condensed nanocrystal array, these bundles may be preserved, because bundles from neighboring nanocrystals can interlock in a gearlike manner.]

To see how this concept explains the remaining features, first consider that the intermolecular "bonds" formed by densely packed surfactant groups on the {111} and {100} facets may imply that the {111} facets can be interconnected not only to {111} facets but also to {100} facets. The latter results in a rotation of the superlattice and formation of the observed $\{100\}_s$ twins (Figure 3). A model for this case is shown in the inset in Figure 3c in correspondence to the experimental observations shown in Figure 3a,c. If one side of the twin preserves a perfect fcc packing, the matching of facets across the boundary will force those on the other side to pack in a way that deviates slightly from the ideal fcc lattice, so that the $[110]_s$ projection of the unit cell may not be perfectly rectangular, as indicated in the idealized model. This corresponds to the experimental observation shown in Figure 3a.

These considerations of the nature of the internanocrystal ordering can be applied to account for the structure of ultrathin (bilayer) TEM specimens of NCAMs, which are frequently found in the $[110]_s$ orientation (Figure 6a), while the more

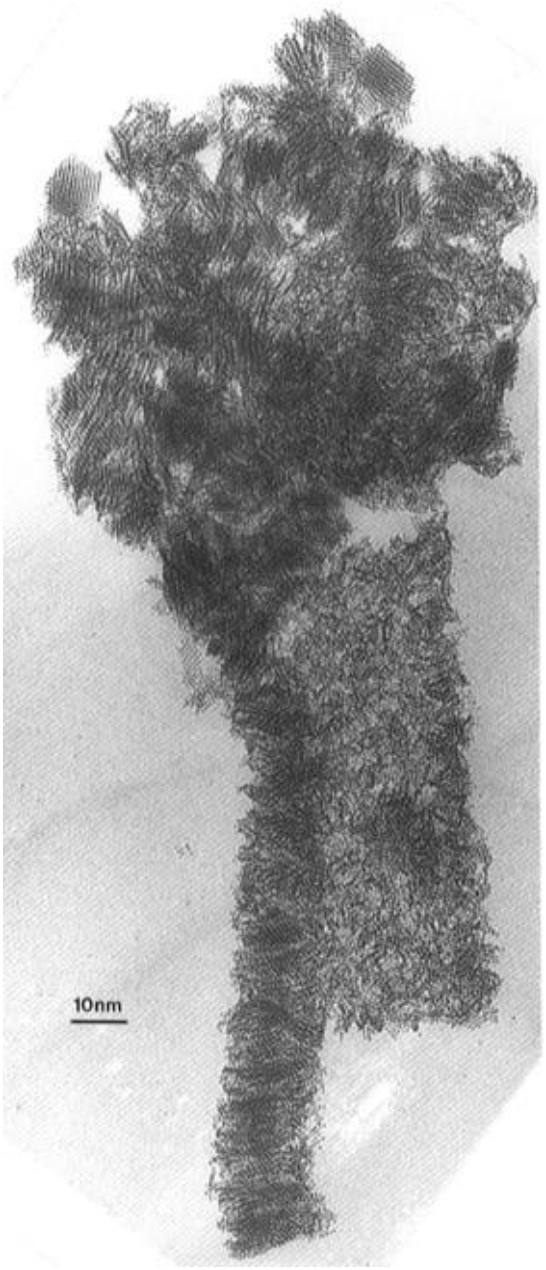

Figure 7. Example of an atypical large aggregate of Ag nanocrystals, which show short-range ordered structure representing a transition from a disordered to an ordered system. Note added in proof: the scale bar should be 100 nm.

compact $[111]_s$ bilayer is hardly ever found. Two domains are observed in this image, one with slightly (8%) smaller nanocrystals, separated by a well-defined grain boundary (GB). The formation of a domain structure reveals how nanocrystals with the same approximate size aggregate preferentially, as is well-known,[20] although the type of segregration observed differs completely from that reported recently by Ohara et al.[22] The surprisingly good alignment of the lattices of the two domains indicates that their formation may be correlated. A striking characteristic of the bilayer packing is that the symmetry can always be described by the projected $[110]_s$ lattice of the 3-D model (Figure 5c, rather than that shown in Figure 5d). To account for this, first note that this image is a projection of the bilayers onto the substrate surface. The film−substrate interaction, which is of diminishing importance for thicker films, evidently orients each TO-faceted nanocrystal so that its [110] axis is normal to the substrate surface, as shown in Figure 6b. This arrangement is well suited to form a $[110]_s$ plane (Figure 5c), which *maximizes* the contact surface area per nanocrystal, because $\{110\}_s$ planes have the lowest (areal) number density, consistent with relatively strong substrate−molecule interactions. By contrast, the high-density fcc-$[111]_s$ growth plane, rarely seen here, may be preferred for weakly faceted (polycrystalline) nanocrystals with close to spherical shapes.

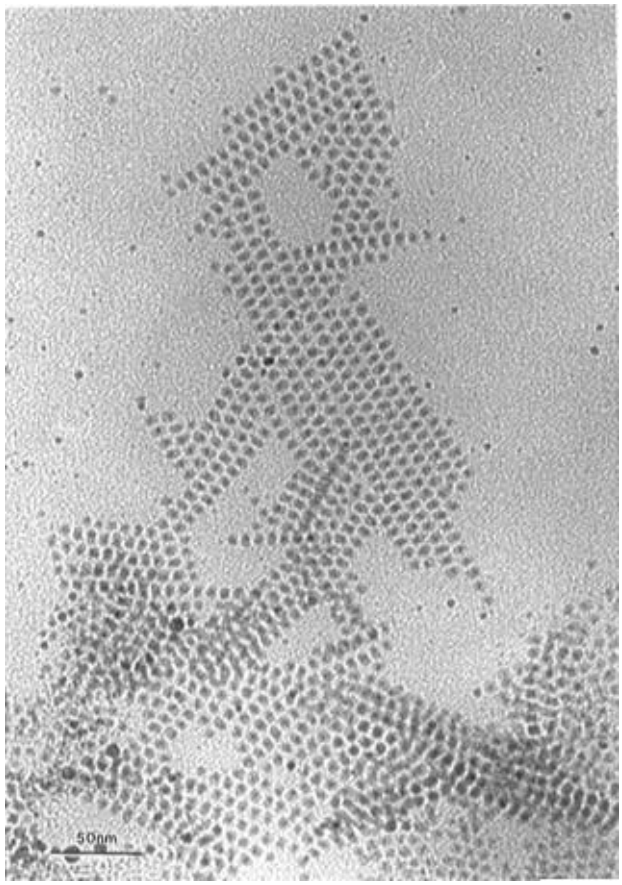

Figure 8. Self-assembled atypical monolayer array assuming a "woodpecker" form.

High orientational ordering should give rise to electron diffraction patterns with regularly spaced intensity maxima on the Ag diffraction ring. The Bragg spots from Ag crystallites can be seen in electron diffraction patterns, but the recorded images are dominated by continuous diffraction rings. This is probably because the recording time for the large diffraction rings is usually longer than 15 s, during which time orientational fluctuations smear the diffraction spots. Under a moderate electron beam dose, such fluctuations are frequently observed, whereas an evolution in *shape* is rarely seen for passivated Ag nanocrystals in this size range. Conventional TEM images are captured using an exposure time shorter than 2 s, so that it is possible to capture the faceted structure of the particles.

Finally, although the structures described above are the most abundant form assumed by these nanocrystals, one can also find certain exotic structures for very thin films, such as the fibrous assembly of aggregates possessing only short-range order shown in Figure 7 and incomplete monolayer structures of highly unusual form (Figure 8). It is not excluded here that under radically different precipitation conditions such forms could predominate.

In conclusion, orientationally ordered molecular Ag−nanocrystal lattices have been observed, their structures have been determined, and a model consistent with the nanocrystal's geometry and bonding (polyhedral shapes and the grouping and interdigitation of surfactant chains) has been proposed to account for the principal structure and its details. These observations

have important consequences: Orientational ordering, which is desirable for so many purposes, occurs readily in such materials, and its microscopic origins can be comprehended. Electronic transport may be described as taking place within an ordered crystalline structure rather than in a granular material. Furthermore, regular channels interconnecting a lattice of uniform voids are intrinsic to these materials; these have a length scale that is interesting with regard to possible applications.

Acknowledgment. The authors thank Dr. Joseph T. Khoury for assistance in preparing the samples, Prof. Janet Hampikian and Dr. Srihari Murthy for assistance with preliminary investigations leading toward this research, and Prof. Uzi Landman and Dr. W. David Luedtke for frequent discussions on their unpublished work on surfactant layers on passivated nanocrystals. Financial support for this research has been provided by the Georgia Tech Research Foundation, the Packard Foundation, and the Office of Naval Research.

References and Notes

(1) deHeer, W. A. *Rev. Mod. Phys.* **1993**, *65*, 611−732. Schmid, G. *Chem. Rev.* **1992**, *92*, 1709.

(2) Fukumi, K.; Chayahara, A.; Kadono, K.; Sakaguchi, T.; Horino, Y.; Miya, M.; Fujii, K.; Hayakawa, J.; Satou, M. *J. Appl. Phys.* **1994**, *75*, 3075−3080.

(3) Terrill, R. H.; et al. *J. Am. Chem. Soc.* **1995**, *117*, 12537. See also: Simon, U.; Schön, G.; Schmid, G. *Angew. Chem., Int. Ed. Engl.* **1993**, *32*, 250.

(4) Brust, M.; Bethell, D.; Schriffin, D. J.; Kiely, C. J. *Adv. Mater.* **1995**, *7*, 795−7.

(5) Dorogi, M.; Gomez, J.; Osifchin, R.; Andres, R. P.; Reifenberger, R. *Phys. Rev.* **1995**, *B52*, 9071−7. Andres, R. P.; Bein, T.; Dorogi, M.; Feng, S.; Henderson, J. I.; Kubiak, C. P.; Mahoney, W.; Osifchin, R. G.; Reifenberger, R. *Science* **1996**, *272*, 1323−5.

(6) First, P.; et al., to be published.

(7) Patil, A. N.; Paithankar, D. Y.; Otsuka, N.; Andres, R. P. *Z. Phys.* **1993**, *D26*,135−7. For review, see: Marks, L. D. *Rep. Prog. Phys.* **1994**, *57*, 603−649.

(8) Cleveland, C.; Landman, U. *J. Chem. Phys.* **1991**, *94*, 7376−7396.

(9) For a recent discussion, see: Reetz, M. T.; Helbig, W.; Quaiser, S. A.; Stimmung, U.; Breuer, N.; Vogel, R. *Science* **1995**, *267*, 367−9.

(10) Whetten, R. L.; Khoury, J. T.; Alvarez, M. M.; Murthy, S.; Vezmar, I.; Wang, Z. L.; Cleveland, C. L.; Luedtke, W. D.; Landman, U. In *Chemical Physics of Fullerenes 5 and 10 Years Later*; Andreoni, W., Ed.; Kluwer: Dordrecht, 1996; pp 475−490.

(11) Murray, C. B.; Kagan, C. R.; Bawendi, M. G. *Science* **1995**, *270*, 1335. For earlier work on "supercrystals", see: Bentzon, M. D.; van Wonterghem, J.; Mørup, S.; Thölén, A.; Koch, C. J. W. *Philos. Mag.* **1989**, *B60*, 169−178.

(12) Whetten, R. L.; Khoury, J. T.; Alvarez, M. M.; Murthy, Srihari; Vezmar, I.; Wang, Z. L.; Stephens, P. W.; Cleveland, C. L.; Luedtke, W. D.; Landman, U. *Adv. Mater.* **1996**, *5*, 428−433.

(13) For example, see: Heiney, P. A.; Fischer, J. E.; McGhie, A. R.; Womanow, W. J.; Denenstein, A. M.; McCauley, J. P.; Smith, A. B. *Phys. Rev. Lett.* **1991**, *66*, 2911−2914.

(14) Whetten, R. L. *Mater. Sci. Eng.* **1993**, *B19*, 8−13.

(15) Luedtke, W. D.; Landman, U. Structure, dynamics, and thermodynamics of passivated gold nanocrystallites and their assemblies. *J. Phys. Chem.*, in press.

(16) Nuzzo, R. G.; Allara, D. L. *J. Am. Chem. Soc.* **1983**, *105*, 4481.

(17) Brust, M.; Walker, M.; Bethell, D.; Schiffrin, D. J.; Whyman, R. *J. Chem. Soc., Chem. Commun*. **1994**, 801.

(18) Alvarez, M. M. Ph.D. Dissertation, UCLA, 1995. See also: Tohno, S.; Itoh, M. *J. Aerosol Sci.* **1993**, *24*, 339−347.

(19) Edinger, K.; Gölzhäuser, A.; Demota, K.; Wöll, Ch.; Grunze, M. *Langmuir* **1993**, *9*, 4. Grunze, M. *Phys. Scr.* **1993**, *T49*, 711−717.

(20) Chemseddine, A.; Weller, H. *Ber. Bunsen-Ges. Phys. Chem.* **1993**, *97*, 636−7. Murray, C. B.; Norris, D. J.; Bawendi, M. G. *J. Am. Chem. Soc.* **1993**, *106*, 6285.

(21) Buffat, P.-A.; Flüeli, M.; Spycher, R.; Stadelmann, P.; Borel, J.-P. *Faraday Discuss.* **1991**, *92*, 173−187.

(22) Ohara, P. C.; Leff, D. V.; Heath, J. R.; Gelbart, W. M. *Phys. Rev. Lett.* **1995**, *75*, 3466−9.

JP961764X